Published in Applied Energy with doi: 10.1016/j.apenergy.2023.121261

A new approach to enhance voltage and frequency stability using an interactive control system for hybrid AC/DC microgrids based-distributed energy resources

*Corresponding author: Khosravi, N,
E-mail: Nimakhosravi64@gmail.com,

Abstract

Overall, voltage and frequency(V/F) stability are essential in microgrids (MGs) to ensure reliable and high-quality power supply for critical loads and to support the integration of renewable energy sources (RESs) while maintaining the stability of the power system. Therefore, V/F stability is particularly important for causes such as load balancing, quality of power supply, renewable energy integration, and grid stability. This study aims to introduce an interactive control system for hybrid MGs (HMGs) based on distributed energy resources (DERs). Here, the defined control strategy objective is to ensure the four system parameters' stability, including voltage/frequency (V/F) and active/reactive (P/Q) power for the units. In this study, the research innovation consists of two layers. The first layer aims to adjust the unit V/F, using an internal voltage and current controller loop combined in the power droop controller (PDC). The second layer is concerned with the steady-state error minimization, created in the first layer due to the droop controller performance. Therefore, the secondary distributed V/F control strategies are designed based on finite-time consensus theory (FTCT) owing to its resistance and stability against various load perturbations and system disturbances, which makes flexible convergence time possible according to different user preferences and operating conditions. The simulation results prove the efficiency of the proposed method strategy. Furthermore, the values of improving the amplitude of oscillations and fluctuations for V/F components vary from 0.02pu-0.2pu and 0.178pu-0.216pu, respectively.

Keywords: Hybrid microgrids, Distributed energy resources, Frequency stability, Voltage stability, Finite-time consensus theory.

Nomenclature

Parameters

SOC	Battery state-of-charge
G	Graph
I	Module current
v_{ci} , v_{co}	Cut-out speeds
t	Time
W_m	Weight matrices
N_s	Number of series connected cells in the module
k_i , k_j	Reactive power share proportion of $unit_i$and $unit_j$
$Pref_i$	Active power reference of $unit_i$
a_{ij}	Component of the proximity matrix '*A*'
T_c	Reference temperature
C	A constant
K	Boltzmann constant value
ω_{i0}^*	No-load frequency of $unit_i$
I_{ph}	Photogenerated current
K	Number of iterations
I_o	Diode reverse saturation current
V	Module voltage
A	Constant value for fixing the curve
R_{sh}	Shunt resistance
E_i^*	Voltage reference of busbar 'i'
L	Laplacian matrix
x_i	Vertex state
w_{ij}	Weighting factor
$\overline{\Delta\omega}$	Average frequency correction
P_i	Active power of $unit_i$
Q_i	Reactive power of $unit_i$
$(a_{ij})_{n\times n}$	Adjacency matrix *A*
E_i , ω_i	V/F domain of $unit_i$
P_{WTG}	Output power of the WT system
P_r	Allowable power
m_i , n_i	ω-*P* and *E*-*Q* droop control coefficients
R_s	Series resistance
e	Electron charge
$\lambda_2, \lambda_3, \lambda_{k+1}$	Constant factors and nonzero
E-*Q*	Voltage-Reactive power
ω-*P*	Frequency-Active power

Abbreviation

AC	Alternating current
ACMG	Alternating current microgrid
BESS	Battery energy storage system
CSC	Current source controller
DC	Direct current
DCMG	Direct current microgrid
DERs	Distributed energy resources
DHC	Distributed hierarchical control
DSFC	Distributed secondary frequency control
DSVC	Distributed secondary voltage control
FTCT	Finite-time consensus theory
FDC	Frequency droop control
FC	Fuel cell
GDAI	Generalized distributed average integration
HMGs	Hybrid microgrids
HPs	Hydropower plants
MGs	Microgrids
MTGs	Micro-turbine generators
PV	Photovoltaic
PDC	Power droop controller
PC	Primary control
PCR	Primary control reserve
PFC	Primary frequency control
REPs	Renewable energy plants
RESs	Renewable energy sources
SFC	Secondary frequency control
SVC	Secondary voltage control
SF	State-feedback
VI	Virtual inertia
VDC	Voltage droop control
VSC	Voltage source controller
VSI	Voltage source inverter
V/F	Voltage/Frequency
WTs	Wind turbines

1. Introduction

The development of renewable energy projects is increasing due to issues such as the cost of fossil fuels, the subject of shortage of these energies in the future, also, more significantly, the discussion of increased weather pollution and reducing the quality of life around the world [1,2]. In the traditional power grid, the energy required for numerous residential, commercial and industrial sites was provided through large energy sources. Some of these consumers were located near concentrated power plants, while others were located farther away from electricity sources. Several backbone technologies form the DERs system, the most prominent of which are photovoltaic (PV), wind turbines (WTs), battery energy storage system (BESS), fuel cell (FC), and micro-turbine generators (MTGs) technologies [3,4]. After the privatization of new power system structures, the arrival of DERs is increasing rapidly. The economic benefits of DERs include two aspects, the landscape of customers and electrical distribution companies [5,6]. For the consumers, this advantage includes reducing energy purchase costs, reducing worries caused by energy rate fluctuations, increasing reliability, improving power quality, etc. On the other hand, for the distribution companies, the mentioned advantages include preventing the increase of network capacity, reducing electrical losses, providing

reactive power, etc. Despite these advantages, these systems also have challenges. First, low voltage networks become passive to active; second, the complexity increases due to the use of converters; Third, DERs with different characteristics, such as hybrid, alternating current (AC), and direct current (DC), cause problems in voltage and frequency regulation. Finally, there are two possible modes of operation, connected to the grid and the island; the mentioned challenge related to DERs infrastructure requires a proper control structure according to which the characteristics of the smart grid can be considered [7,8].

Due to the flexibility of controlling the interface inverters used in the MG structure, the MG control and operation also become more flexible [9]. Nowadays, the development and operation of MGs in the HMGs form have significantly increased due to the exercise of all available energy production sources [10,11]. Therefore, the nature of the control of MGs will be a significant challenge for experts in this field, considering the issue of the integration of different devices. In this regard, the control system of an HMG, depending on its output (controllable or uncontrollable), includes three levels; primary, secondary, and tertiary [12]. The primary level of control can be designed based on a voltage source controller (VSC) or current source controller (CSC). This system control level is independent and via local measures ensures the stability of the MG in different operating conditions. At the secondary level, 'V/F' droop control (VDC/FDC) is designed for stability. In the sense that events such as changing operating mode, load change, and even the occurrence of errors can cause a steady-state error in the fundamental MG variables. The application of tertiary-level control is for wide MGs with several voltage-controllable sources. Therefore, it is necessary to use a master control system to create coordination in the MGs. The task of this system is to control the power management in the MGs [13].

The problem of controlling the MGs has been previously addressed with different techniques; see e.g. [14] where the impact of several operating strategies for BESS to provide primary control reserve (PCR) is presented. This study presents a case study of a 2 MWh BESS under the German regulatory framework for various parameters such as energy exchange with scheduled transactions, total energy turnover, full cycle equivalence, and state of charge distribution. Examine the impact of operational strategies. However, based on the real samples, the effects of multiple factors containing the governor ratio, governor dead band, droop rate, and quick load response may not be suitable for the PCR method. In [15], an initial state-feedback (SF) strategy has been suggested for MGs to improve their transient behavior in both islanded and connect to grid modes. The influence of the approach is evaluated by time-domain simulations on a CIGRE standard medium-voltage distribution grid with three DERs units. Although, the main disadvantage of the SF method is that the disturbance enters into the process and upsets it. In [16], a comprehensive method for improving voltage and primary frequency control (PFC) in HMGs is modeled. As for island operation, the proposed procedure results in an efficient autonomous power-sharing task by link converters. In [17], the authors develop a new alternative control law, called generalized distributed average integration (GDAI), to set secondary control goals, namely steady-state precision frequency recovery and balanced power sharing in the existence of clock drift achieved. However, the time delay of communication within the network is not incorporated into the GDAI control method, just as the temporal variation of the voltage amplitude was not analyzed in this study. The influence of the communication system on the secondary control power of ACMG during independent operation has been investigated in [18], where a stochastic delay model of the industrial communication protocol at the secondary control matched is combined with that of the MG simulation. In [19,20], the structure and architecture of secondary control are presented extensively in the form of a review. An approach based on distributed tertiary control of DCMG clusters is discussed in [21]. The suggested control mechanism operates a participatory process to set voltage regulation for MGs. While the voltage regulation policy manages the load distribution among the MGs in each cluster at a lower level, wherein each MG carries a communication network connected to the secondary control system. Experimental analyses on two group layouts demonstrate superior control undertaking and validate stability to transducer losses and communication failures. However, considering the dynamics of the problem, the complexity of the proposed method is quite noticeable. In [22], an optimization method has been developed for energy management at the tertiary level for several MGs. The various connection models and settings of the secondary level controller are determined using the binary gray wolf optimization in the software platform. The results show that under the proposed method,

compared to the island state, the operating costs can be reduced by 62.91%. Nevertheless, as the implementation time duration is often limited, meta-heuristic algorithms may not perform positively.

The effect of large-scale PV, WT, and hydropower plants (HPs) on the V/F stability of the Jordanian national grid has been investigated in [23]. The study shows that the introduction of backup voltage and reactive power can double the full power of renewable energy plants (REPs). An analysis of the grid frequency stability shows that the latter can be held when the penetration level of REP gains 40% of the total output. In addition, this investigation has demonstrated the significance of connecting to adjoining power systems. However, the cost of HPs is not cost-effective. A novel wide-area adaptive load-shedding technique for the practical recovery of power system V/F stabilities has been developed in [24]. Although this method shows an adequate response, it is represented by a high computational load. On the other hand, it may cause power outages for some consumers. In [25], a game theoretic approach has been proposed to support the frequency stability in the MG, utilizing a hybrid of energy storage systems and load-shedding strategies. The power system frequency resilience in virtual inertia (VI)operating from inverter-based DERs is analyzed in [26], where the state-space sample for the virtual power system grid with 'VI' developed as a feedback control loop. The outcomes show that the optimal distribution remarkably enhances the system frequency resilience by reducing the frequency change rate and delaying it. However, the mentioned topology cannot be executed in island modes where the 'VI' unit has to work as a grid-forming unit. In [27], a robust iterative learning controller has been designed for voltage and frequency stabilization of HMG. Moreover, a strategy based on P-F, Q-V droop control has been proposed in [28] to improve the system stability. In previous studies some of them focused on only one level control design [14,15,16,17,18,19], others based on the metaheuristic algorithms that lead to computing time delays and need powerful calculation devices [11,13,21,22]. On the other hand, some existing methods can operate just in island mode as well as cause power outages for some consumers [25].

The present paper is devoted to the control of hybrid microgrids (HMGs) based on distributed energy resources (DERs). For this considered system, we propose a two-layer control structure for DERs (units). The first layer (PDC) is designed based on two-control loop including VDC and FDC in order to adjust the units V/F. While, the second layer is constructed using FTCT technique in order to eliminate the steady-state error generated by the first layer and to guarantee the stability of the desired V/F in nominal values for each perturbation and oscillation. The main contributions of the present paper are summarized below:

- FTCT protocol is provided for FDC restoration, VDC stabilization concerns, and active power sharing between connected inverters.

- Implement a reliable second-order control scheme for island HMGs using distributed cooperative control of multi-agent systems. Thus, an individual inverter only needs local information and details about its adjacent system in the omnidirectional communication network. Therefore, the suggested technique is thoroughly distributed.

- Compared with traditional distributed controllers, the proposed technique reaches agreement quickly and exhibits more accurate and robust execution against controller activation, reconfiguration, and load changes.

- The case study examines the plug-and-play resilience and scalability of the suggested ordered distributed control approach.

- The operation and working conditions of the individual HMGs will certainly not be constant and stable and may undergo various changes. In the proposed technique two stability constraints (a distributed secondary V/F control strategy based on the FTCT) have been considered. Furthermore, steady situations stand achieved by supporting and maintaining the scheduled limits. With varying operational requirements or malfunctions, the controller parameters automatically adapt to the new conditions.

The rest of the paper is organized as follows. Section 2 provides the HMG description and modeling. Section 3 presents the proposed method description. Section 4 discusses the simulation results, and Section 5 concludes this paper.

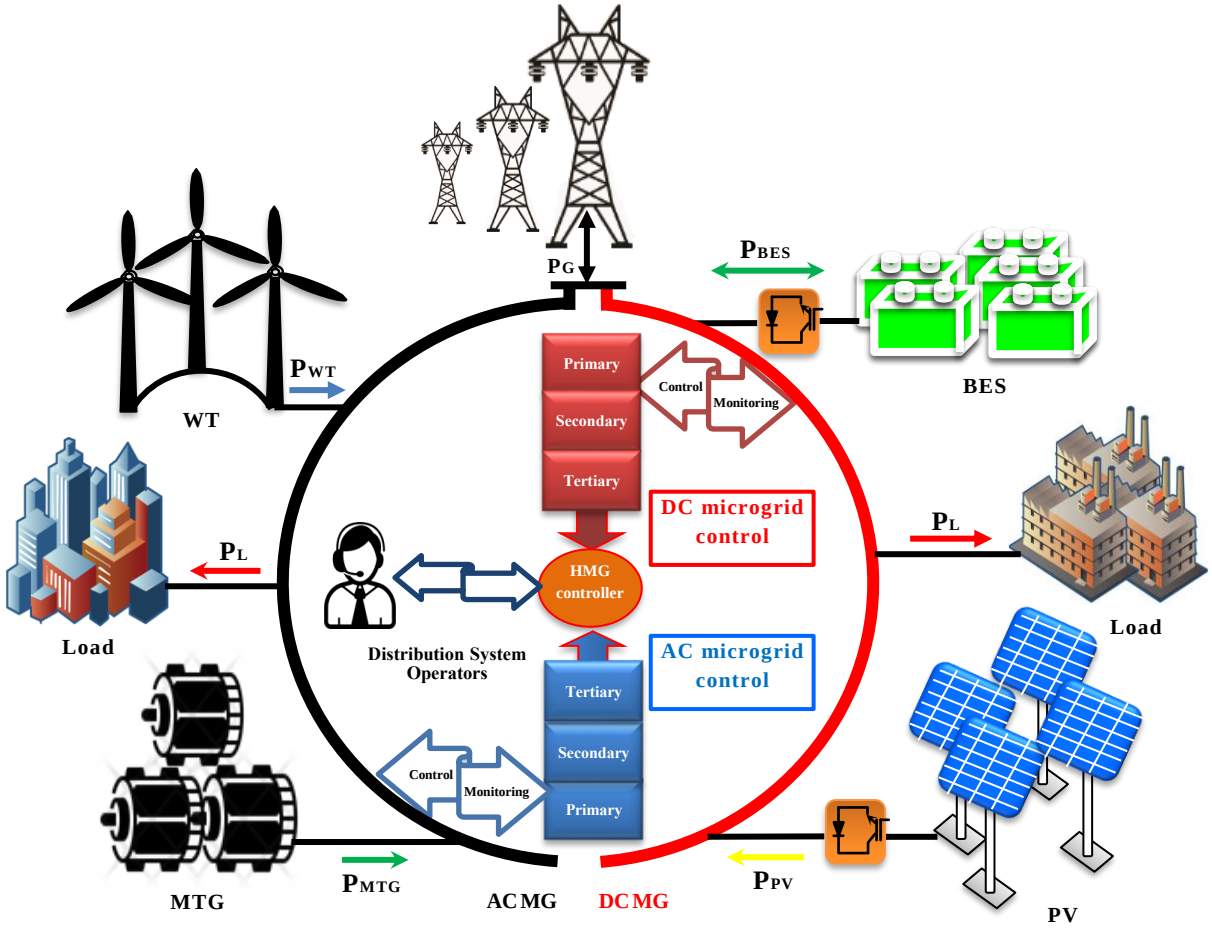

Fig.1. The structure of HMG

2. HMG description and modeling

DERs are ordinarily operated on the MGs platform. On the other hand, the utilization of MGs in the form of a hybrid format (HMG), due to the diversity of electricity generation, has received more attention from industry experts. The HMG consists of two systems of separate nature that can be properly operated by some devices based on power electronics to supply loads of different nature (AC or DC). The structure of an HMG is shown in Fig. 1. Since the case study is an HMG based on DERs, in the following, some generating systems applied in HMG will be briefly introduced.

2.1 Solar system

PVs, which convert sunlight into electricity, is a key component of microgrid systems because they provide a clean, renewable source of energy. In addition, PVs are modular, meaning that they can be easily added or removed from a microgrid system depending on the energy needs of the community. This makes PVs a flexible and scalable solution for microgrid systems. In a typical microgrid system, PVs are connected to batteries or other energy storage devices,

which allow the system to store excess energy generated during periods of high sunlight and use that energy during periods of low sunlight. PVs can also be connected to other types of renewable energy sources such as wind turbines or hydroelectric generators to provide a more robust and reliable source of electricity for the microgrid. PV systems consist of several modules that are placed in series or parallel to produce the output power with the desired voltage and current. The types of PV models and complete comparison between them have been studied in [29,30]. In recent years, PV is expanding due to suitable operating efficiency, low maintenance costs, lack of greenhouse gas emissions, and environmental compatibility. Fig.2 shows the single-diode equivalent circuit of a PV cell and the relationship between the current and voltage at the terminals of the PV cell will be obtained from equation (1) and (2).

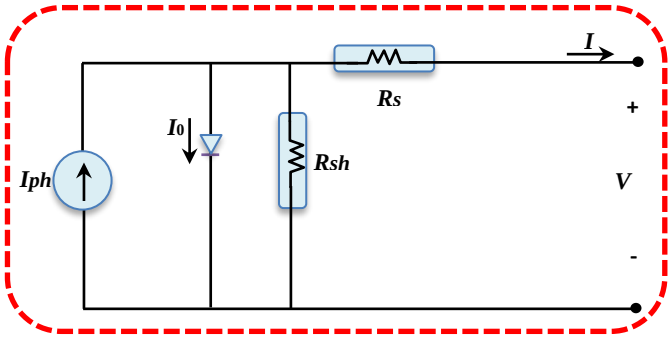

Fig.2. PV equivalent circuit

$$I = I_{ph} - I_o[\exp((V + IR_s)/(N_s V)) - 1] - (V + IR_s)/R_{sh} \quad (1)$$

$$V = (AKT_c/e)\, ln\big((I_{ph} + I_0 - I)/I_0\big) - R_s I \quad (2)$$

where I is the module current, V is the module voltage, I_{ph} is the photogenerated current, I_0 is the diode reverse saturation current, R_s is the series resistance, R_{sh} is the shunt resistance, N_s is the number of series connected cells in the module, A is a constant value for fixing the curve, e is the electron charge ($1.602\times 10^{-19}C$), K is the Boltzmann constant value ($1.38\times 10^{-23}\frac{j}{k}$), and T_c is the reference temperature (25c) PV cell.

2.2 BES system

Batteries, flywheels, and supercapacitors are among the energy storage devices operated in MGs. One of the applications of these devices is to balance power between loads and energy sources; in other words, sometimes these devices are operated in the MG when the power output of resources does not match with loads. Energy storage units are dependent on electronic power converters for connecting to the grid, similar to some DERs. These converters have a bidirectional operation for energy storage and discharge [31, 32]. The state-of-charge for a battery at time (t) can be indicated using the following equation:

$$SOC(t) = SOC(t-1) + \int_0^t (I/C_{bat}).dt \quad (3)$$

where SOC is battery state-of-charge at time t (%), $SOC(t-1)$ is battery initial state-of-charge (%), I will be charge/discharge current (A), t is time (h), C_{bat} is battery capacity (Ah), respectively. The global BESS installation capacity is shown in Fig.3.

2.3 WT system

WT is one of the considerably widely used power generation devices in the MG system. One of the main advantages of WTS in microgrid systems is that they can provide a stable and consistent source of power, as long as there is

enough wind. This is particularly useful in remote or isolated areas, where access to the main power grid may be limited or unreliable. WTs can also help to reduce the carbon footprint of microgrid systems, as they produce clean, renewable energy that does not emit greenhouse gases. This can be particularly important in areas where there is a high demand for energy, but limited access to traditional energy sources. WT production capacity depends on various factors such as wind regime, wind speed, air density, blade angle, tower height, turbine efficiency, gearbox, generator, etc. Installed capacity, the volume of energy produced by wind farms during the years 2000-2020, is shown in Fig. 4. The relationship between wind turbine production capacity and wind speed is as follows:

$$P_{WTG}\big(v(t)\big) = \begin{cases} 0, & v(t) < v_{ci} \\ \frac{v(t)-v_{ci}}{v_r-v_{ci}} \times P_r, & v_{ci} < v(t) < v_r \\ P_r & v_r < v(t) < v_{co} \\ 0, & v(t) > v_{co} \end{cases} \quad (4)$$

where P_r is the allowable power, v_{ci} and v_{co} are the cut-out speeds, and P_{WTG} is the output power of the WT system [33].

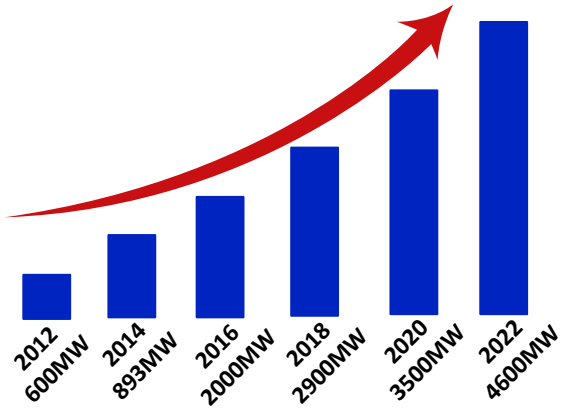

Fig.3. Global BESS application scale in recent years

2.4 MTG system

MTGs have found a remarkable place in MGs due to their control flexibility and high response speed. These appliances have been operated in low production capacities (25kW to 500kW) as one of the energy supplies sources in the DERs [34].

3. The proposed method description

Operating power grids with high power output fluctuations, such as PV (due to atmosphere oscillations), and WT (due to wind oscillations), will always be a principal challenge, particularly when energy demand exceeds production. Therefore, the case study includes four energy production systems with different natures, which include $unit_A$, $unit_B$, $unit_C$, and $unit_D$ respectively. Dynamic parameters of units are shown in Table 1.

As mentioned earlier, a hierarchical control approach is proposed for DERs (units). It is assumed that the operation of the proposed case study will be performed to three-phase impedance balanced units. Fig. 5, shows the control configuration diagram of the proposed approach. The two proposed control layers for the case studies will be defined as follows:

i. First-layer: The first-order (ω-P , E-Q) droop control will be extended to generate the V/F signals for the unit inverter controller's components (interior voltage and current), therefore the unit can fast respond to load variation and load oscillations, and carrying out efficaciously adjustment of unit components (V/F).

ii. Second-layer: The FTCT-based secondary distributed control is developed to bound the unit components (V/F) variations exited from the PDC, and the suitable reactive power required distribution between all units.

Before describing the objective control modes, defined above, the topic of FTCT, which is an essential element in solving the problem, will be discussed first. In the following, two control topics including VDC and FDC in the primary level will be comprehensively explained. Then, in the next part, the distributed SFC and SVC (DSFC-DSVC) modes in the secondary mode control will be examined. According to this theory, the structure of a system with n nodes will be modeled by the graph:

$$G = (V, E) \tag{5}$$

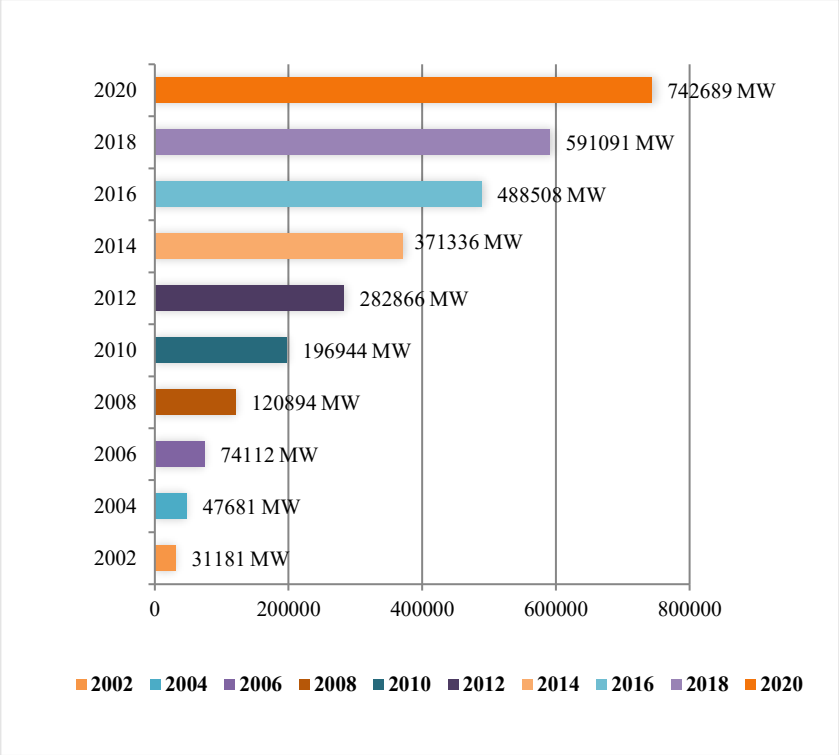

Fig.4. Installed capacity of wind turbines worldwide

In relation (5); V=$(v_1, v_2, .., v_n)$ and E=$(e_1, e_2, \dots, e_n)$. Each of the parameters describes the adjustment of boundaries for couples of unordered vertexes [35-39]. Graph G with n vertices is defined by an adjacency matrix A with features indicated as $(a_{ij})_{n\times n}$, where $a_{ij} = 1$ if v_i is adjacent to v_j, and a_{ij} = 0 otherwise. The Laplacian matrix $\boldsymbol{L}$= (l_{ij}) of the graph (G) will be described as

$$\begin{cases} l_{ij} = \sum_{i\neq j} a_{ij} = d_i \\ \quad l_{ij} = -a_{ij} \end{cases} \tag{6}$$

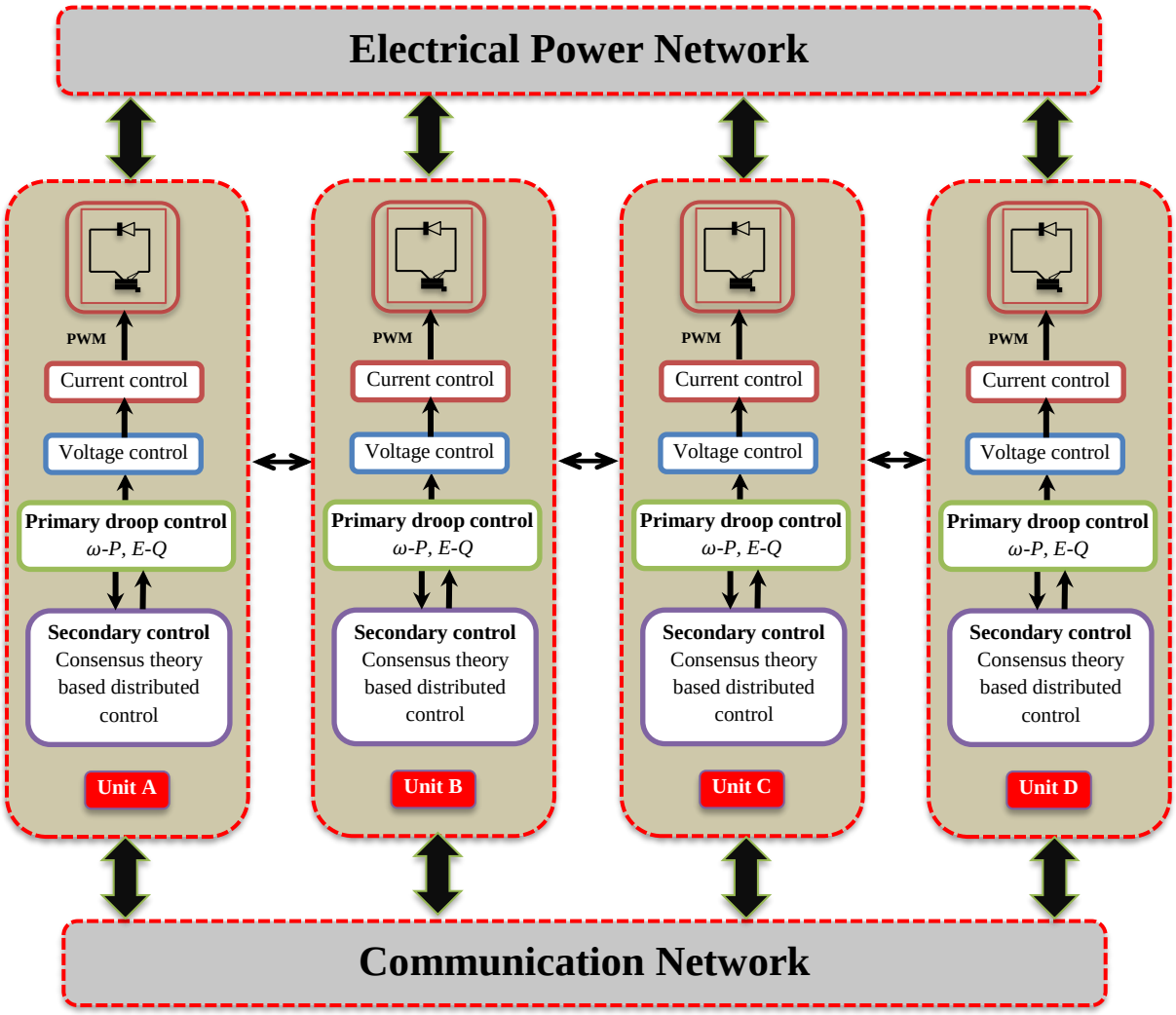

Fig.5. The proposed DHC diagram

In the following, the proposed strategy based on FTCT is expressed as follows:

$$\mathrm{x}_i(k+1) = \sum_{j\epsilon N_i} w_{ij}(k)x_j(k), i = 1,2,\dots,n \qquad (7)$$

where x_i represents the vertex state (v_i), including unit bus V/F, and load demands in the MG; k is the number of iterations; w_{ij} is the weighting factor. By setting a set of weight matrices $W_m = I - 1/(\lambda_{m+1})L$, m= 1,2…, k with:

$$w_{ij}(m) = \begin{cases} 1 - d_i/(\lambda_{m+1}) & j = 1 \\ 1/(\lambda_{m+1}) & j \in N_i, m = 1,2,\dots,k \\ 0, otherwise \end{cases} \qquad (8)$$

where $\lambda_2 \neq \lambda_3 \neq \lambda_{k+1} \neq 0$ represent the k different non-zero eigenvalues of the Laplacian matrix L. The states of all vertices will converge to the average of the initial state within k iterations by the below relation:

$$\mathrm{x}_1(k) = x_2(k) = \cdots, x_n(k) = 1/n \sum_{j=1}^{n} x_j(0) \qquad (9)$$

TABLE 1 Dynamic parameters of units

Parameters	Symbol	Unit	Value
Filter inductance	L_f	mH	0.15
Filter capacitor	C_f	μF	760
Switching frequency	f_s	kHz	10
Rated frequency	ω_0^*	rad/s	100π
Line impedance	Z_A	Ω	0.03 + j0.02
Line impedance	Z_B	Ω	0.04 + j0.03
Line impedance	Z_C	Ω	0.05 + j0.04
Line impedance	Z_D	Ω	0.04 + j0.03

3.1 FDC and VDC in the primary layer

DERs are separated into two main disciplines in terms of controllability. The units with controllable output (MTG, FC, etc.), and the units with uncontrollable output (PVs, WTs, etc.). Therefore needed, intended for each mentioned energy source, is an appropriate primary control (PC) system [40,41,42]. The PC, as the heading signifies, acts quickly, and is the first control layer that operates when the perturbation occurs, preventing instability of output and consequent units. This level of control is separated into two main categories. This control system according to the unit capacity and the set point sent by the operator (central controller) produces a constant power. The voltage source inverter (VSI) is the makeup of a DC voltage source, a three-phase full-bridge inverter, and an LC filter. Fig. 6 shows the specific configuration, containing an external loop power controller and an internal double-loop voltage-current controller, which stands assumed for the PDC in this analysis. A more description of the multi-loop controller structure can be found in [43,44,45]. Non-Gaussian noises are one of the influential factors in measuring parameters. According to the proposed technique, is no need for state estimation techniques based on the KF-based main path algorithms to deal with non-Gaussian noises. Some drawbacks of these algorithms include complexity, low measure speed and accuracy, the absence of resistance to measurement errors, and the sensitivity to system sizes. More details regarding dealing with the cited noises are provided in the literature [46,47,48]. The PDC applied to dynamically modify the MG load demands between numerous units by the voltage-reactive power (*E*-*Q*) and frequency-active power (ω-*P*) droop features:

$$\begin{cases} \omega_i = \omega_i^* - m_i\left(P_i - P_{ref_i}\right) = \omega_{i0}^* - m_i P_i \\ E_i = E_i^* - n_i Q_i \end{cases} \tag{10}$$

where E_i and ω_i are the V/F domain of $unit_i$, respectively; ω_i^*(100π(rad/s)) is the ordered frequency of $unit_i$, ω_{i0}^*=ω_i^*+$m_i P_{ref_i}$ is the no-load frequency of $unit_i$; E_i^* is the voltage reference of busbar 'i'; m_i and n_i are the ω-*P* and *E*-*Q* droop control coefficients, respectively; P_i is active power and Q_i is reactive power of the $unit_i$; P_{ref_i} is the active power reference of $unit_i$. To facilitate the arrangement of the SFC and make the no-load frequency match (for P_i = 0 in (6)), the ω-*P* droop coefficient m_i is developed to meet the following equation:

$$m_1 P_{ref_1} = m_2 P_{ref_2} = m_3 P_{ref_3} = m_4 P_{ref_4} = C \tag{11}$$

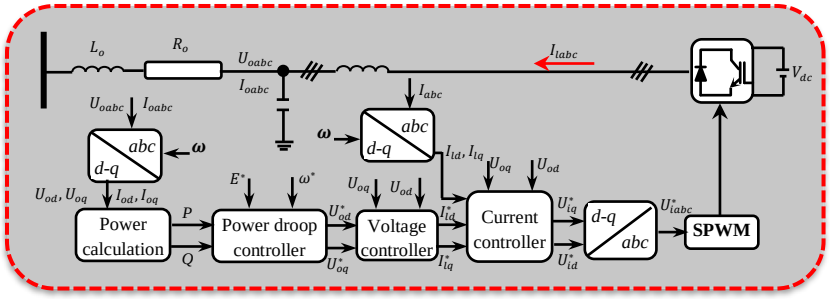

Fig.6. Diagram of the PDC

where *C* is a constant. According to (11), the *ω-P* droop control factor of the individual unit can be regulated based on the optimal active power authority (reference) P_{ref_i}defined by the second-layer. The *Q-E* droop control factor for the individual units will be revamped by (20) in the next part.

3.2 DSFC and DSVC in the secondary layer

In an electrical grid, the frequency of the power system is a crucial parameter that must be maintained within a narrow range for the grid to operate reliably. Distributed SFC involves the use of decentralized control algorithms to adjust the power output of individual generators in response to changes in the system frequency. This helps to restore the system frequency to its nominal value after disturbances such as sudden load changes or generator failures. Voltage control is another critical aspect of power system operation. The voltage levels in the system must be kept within acceptable limits to ensure the safe and efficient operation of electrical equipment. Distributed SVC involves the use of decentralized algorithms to adjust the reactive power output of generators and other reactive power sources in response to changes in the system voltage. This helps to maintain the system voltage within acceptable limits, even during times of high demand or other disturbances. In the case study structure, due to the presence of a droop controller, in the steady-state, the voltage and frequency of the unit are not exactly equal to the nominal values, and a steady-state error occurs in the voltage and frequency of the units. Based on the challenges mentioned the proposed approach for the secondary layer consists of two modes. The first control mode will include distributed SFC. As it turns out, $unit_A$ and $unit_B$ are operating synchronously at points α and β at the frequency ω^*. State changes from α and β to γ and δ occur when the load demand fluctuates positively, so the power output will increase to the points indicated by the PDC. By making the above changes, the system frequency (unit) will be reduced to the frequency ω. To recover ω to the value of ω^*, the operating points of $unit_A$ and $unit_B$ move from points γ and δ to points ε and ξ, respectively, by shifting the PDC curves. Therefore, modifying the operating frequency of the system to the nominal frequency will be possible by implementing the first control mode at the secondary level. If the slopes of the *ω-P* droop control for $unit_A$and $unit_B$are $D_1$and D_2, the frequency compensation $\Delta\omega_i$can be expressed as:

$$\Delta\omega_i = \omega_i^* - \omega_i = D_i\left(P_i - P_{ref_i}\right) \tag{12}$$

Given that the measured noise from the system voltage and current will cause problems such as frequency fluctuations, overshoot, etc.; To overcome the above issues; average frequency correction $\overline{\Delta\omega}$ is considered the correction signal for any unit.

$$\overline{\Delta\omega} = 1/n\sum_{i=1}^{n}\Delta\omega_i = 1/n\sum_{i=1}^{n}D_i\left(P_i - P_{ref_i}\right) \tag{13}$$

where $\overline{\Delta\omega}$ can be calculated using (9) based on the FTCT for sharing the frequency compensation $\Delta\omega_j$ among adjacent units.

$$\Delta\omega_i(k+1) = \sum_{j\epsilon N_i} w_{ij}(k)\Delta\omega_i(k), i = 1,2,\dots,n \tag{14}$$

The average frequency compensation by considering the proposed algorithm (FTCT) will be obtained from the following relation:

$$\Delta\omega_1(k) = \Delta\omega_2(k) = \cdots = \Delta\omega_n(k) = 1/n\sum_{j=1}^{n}\Delta\omega_j(0) = \overline{\Delta\omega} \tag{15}$$

Finally, the proposed distributed SFC relation interlinked with the PDC as follows:

$$\omega_i = \omega_i^* - D_{ref_i}P_i + \Delta\omega_i \tag{16}$$

The proposed DSFC structure is presented in part (a) of Fig.7. The next topic is the reactive power control and DSVC, which is shown in part (b) of Fig. 7. On the other hand, since the unit voltage is a local variable and has different values in different busbars, it's not possible to achieve a balanced distribution of reactive power between units simply by relying on *Q-E* droop control. To restore the system V/F to the nominal values and amends for the steady-state error generated by the droop control, the SVC, reactive power, and frequency be added to the VSC. According to the relations (6-9) provided for FTCT, $Unit_j$ exchanges its voltage U_{oj} with the adjacent units locally:

$$U_{oi}(k+1) = \sum_{j \epsilon N_i} w_{ij}(k) U_{oj}(k), i = 1,2,\dots,n \qquad (17)$$

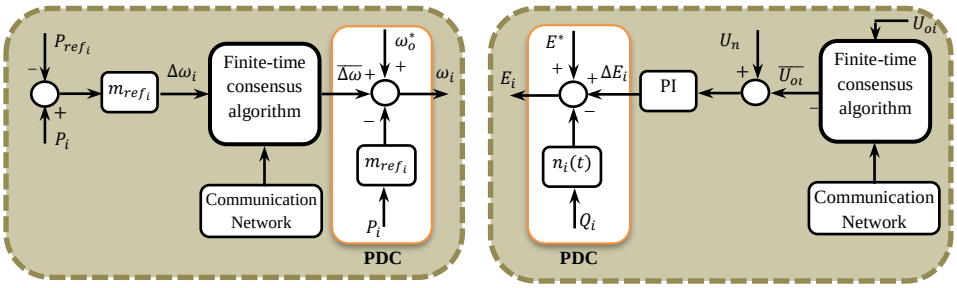

Fig.7. Block of the distributed secondary control (a) DSFC mode (b) DSVC mode

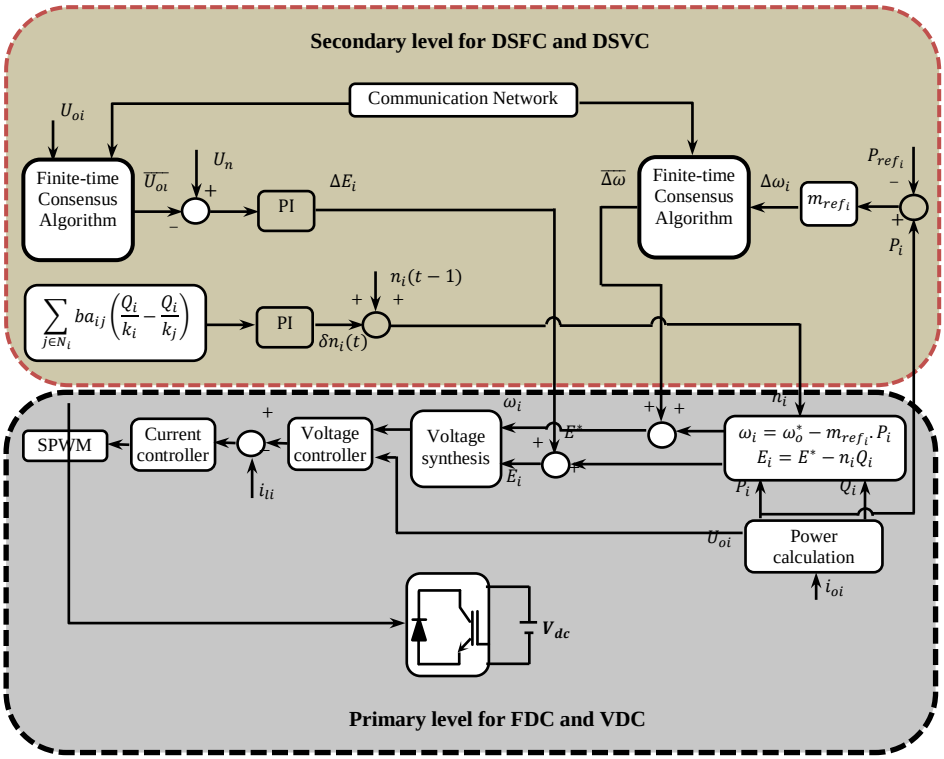

Fig. 8. The proposed DHC structure

Using the distribution communication network applied to the DSFC in Fig. 7(a), the relation (17) can furthermore assemble to a harmony significance within *K* iterations as

$$U_{o1}(K) = U_{o2}(K) = \cdots = U_{on}(K) = 1/n \sum_{j=1}^{n} U_{oj}(0) = \overline{U_o} \qquad (18)$$

In the following, each unit deals with the reactive power allocation proportion and reactive power Q_i of $unit_i$ with its neighboring units and then acquires the variation coefficient Δn_i by the following relation.

$$\Delta n_i = \sum_{j \epsilon N_i} ba_{ij}\left(Q_i/k_i - Q_i/k_j\right)\Delta\omega_i(k), i = 1,2,\dots,n \quad (19)$$

where 'b' is the gain coefficient; a_{ij} is the component of the proximity matrix 'A' of a communication network; k_i and k_j are the reactive power share proportion of $unit_i$and $unit_j$, which stand determined according to the ordered reactive power of DG 'i' and 'j'. Further, Δn_i is passed to the PI controller H_i(s) for computing the revision delta(t). The *Q-E* droop factor is corrected as follows:

$$n_i(t) = n_i(t-1) + \delta n_i(t) \quad (20)$$

The suggested distributed secondary *Q-E* components control is combined with the PDC as follows:

$$E_i = E_i^* - n_i(t)Q_i + \Delta E_i \quad (21)$$

TABLE 2 Units PI controller parameters

Parameters	$\mathbf{Unit}_A$	$\mathbf{Unit}_B$	$\mathbf{Unit}_C$	$\mathbf{Unit}_D$
$G_i(s)$ proportional gain	5	5	5	5
$G_i(s)$ integral gain	50	50	50	50
$H_i(s)$ proportional gain	0.08	0.08	0.08	0.08
$H_i(s)$ integral gain	1.9	1.9	1.9	1.9

In this section, the proposed control approach for the case study is defined. This approach is summarized in two control levels, including primary and secondary levels. The primary layer followed by the PDC index consists of two control structures (VDC and FDC). FDC and VDC factors in PDC when perturbations occur, quickly and as the first control layer is activated and prevents the unit from becoming unstable. Due to the presence of a droop controller, in the steady-state, the voltage and frequency of the unit are not exactly equal to the nominal values, and a steady-state error occurs in the voltage and frequency of the unit. For this objective, in the secondary layer, by two control modes, SFC and SVC, utilizing the FTCT technique, it will be possible to recover and reduce the amplitude of frequency and voltage oscillations of the system. An overview of the proposed method in the form of a distributed hierarchical control (DHC) is shown in Fig. 8. The PI controller parameters of units are listed in Table 2.

4. Simulation results

As presented earlier, the case under study consists of four units. The operating conditions of the units considered as an island. The case study has been implemented along with the proposed method in MATLAB software. How this study can be extended in practical applications is as follows:

In practice, this method can be implemented using a digital card, such as the dspace1104 card. Programming is carryout operating the SIMULINK modeling implement, which allows graphically posing the problem utilizing interconnected blocks. Numerous DSP-based real-time consequence designs currently reach an interface to Simulink, via which they can transform the Simulink blocks into machine code that can be performed on a DSP-based system. This greatly reduces the development and prototyping time for the control of prototyping time for system control. There are three steps to prototyping:

- Construction of the control system using Simulink blocks.
- Simulation of the system to see the results in different scenarios.
- Run the prototype in real-time via the DS1104 board.

To facilitate understanding of the output results, parameters such as voltage, active and reactive power, each of the above components are presented in the form of a per-unit system. In this section, the results will be defined according to the objective functions, including the dynamic behavior of voltage and frequency of the system in the defined

operating conditions, along with the two parameters of active and reactive power of case study components (units), respectively. Operation is considered according to the implementation of the proposed method (distributed hierarchical control using FTCT) and the conventional method. Fig. 9, shows the voltage output of $unit_A$. This plot consists of two outputs with and without the proposed method. As shown in Fig.9, the voltage of $unit_A$ has a fluctuation with a relatively high amplitude (0.03pu) which will then have a decreasing trend. As the system continues to operate, the voltage output will normally increase to 0.985pu, but this value will fluctuate by 0.004pu. Then, using the proposed method, according to the compensation and determination of appropriate coefficients, the system voltage is in a profitable state, and the amplitude of fluctuations of the mentioned component will be nearly zero; in addition, the final value of the mains voltage will be stabilized in 1pu with an increase of 0.013pu.

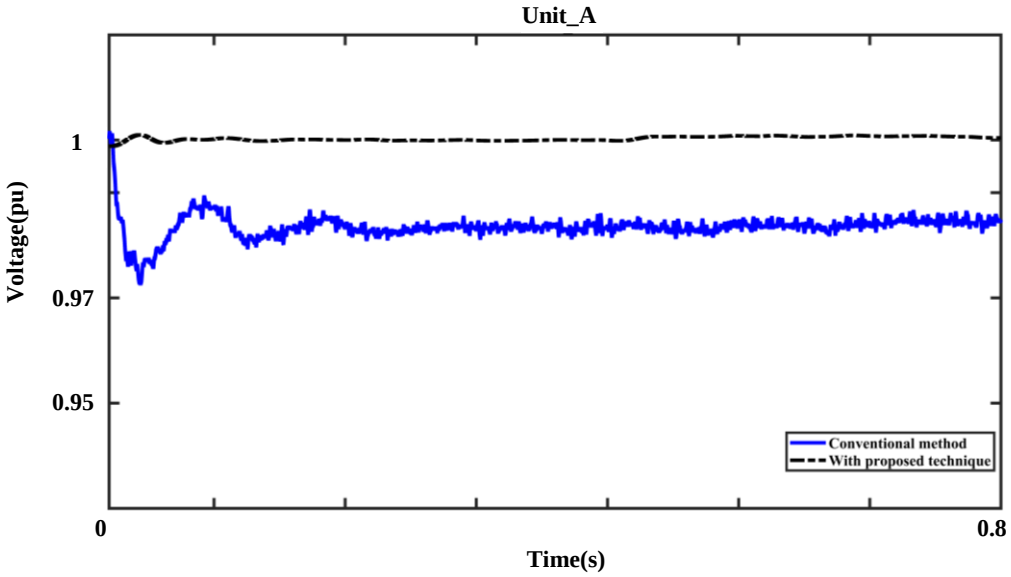

Fig.9. The voltage output of $unit_A$ with and without operating the proposed method

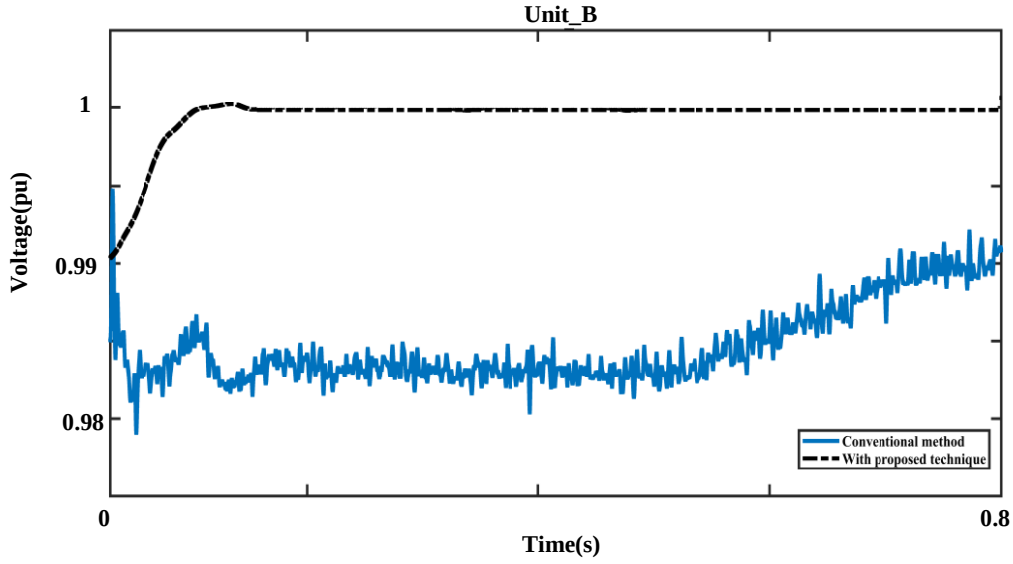

Fig.10. The voltage output of $unit_B$ with and without operating the proposed method

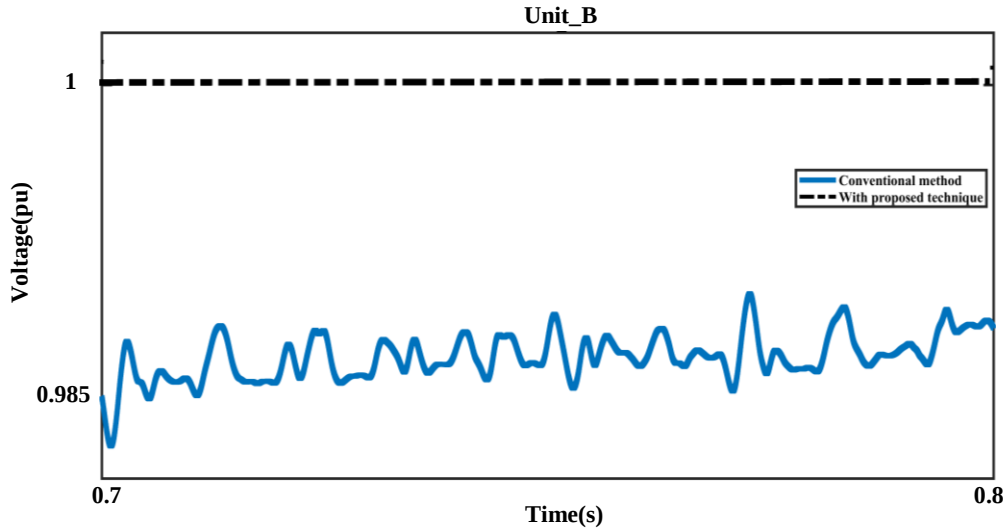

Fig.11. The open view of $unit_B$ voltage, with and without operating the proposed method

The $unit_B$ output voltage is shown in Fig. 10. The voltage waveform of this unit normally has a noticeable oscillation (0.989pu to 0.992pu) in the form of instability, despite reaching the required quorum, which is visible in the magnified part. On the other hand, the mentioned oscillation of the desired system will be improved to an acceptable level by considering the proposed method, and finally, the voltage parameter will be stabilized at a nominal value of 1pu. Fig. 11 shows the open view of the desired unit (B) voltage fluctuation value during 0 to 0.1 seconds. Certainly, non-Gaussian noises, including Laplacian and Cauchy distribution noises, can be influential factors in the output of parameters. Generally, the conventional methods to deal with the mentioned noises are estimation techniques based on Kalman filters. In the heavy-tailed non-Gaussian noises, the tails are not exponentially determined. Unlike the bell curve with a normal distribution, heavy-tailed distributions reach zero at a slow velocity and can include outliers with extremely high values.

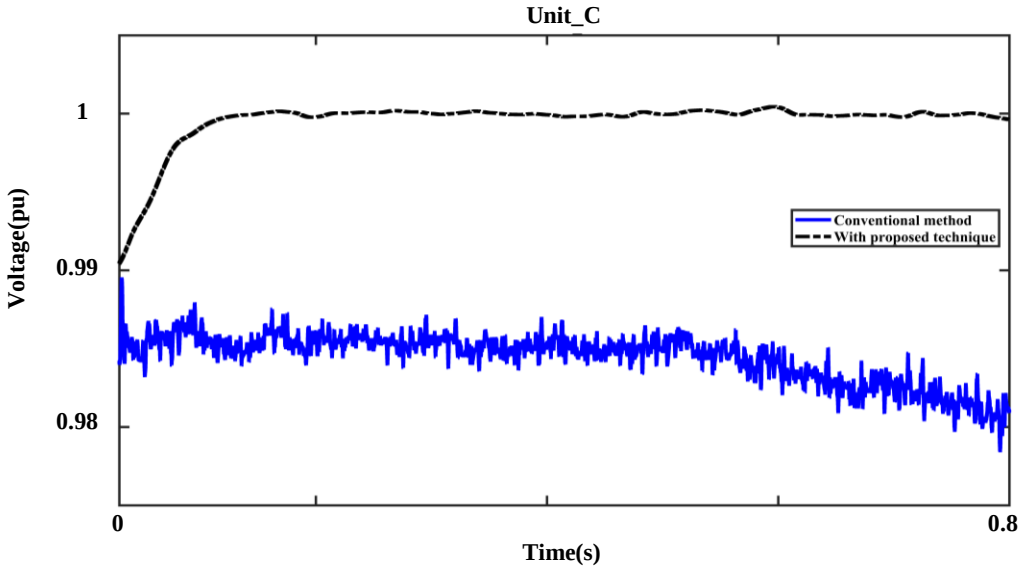

Fig.12. The voltage output of $unit_C$ with and without operating the proposed method

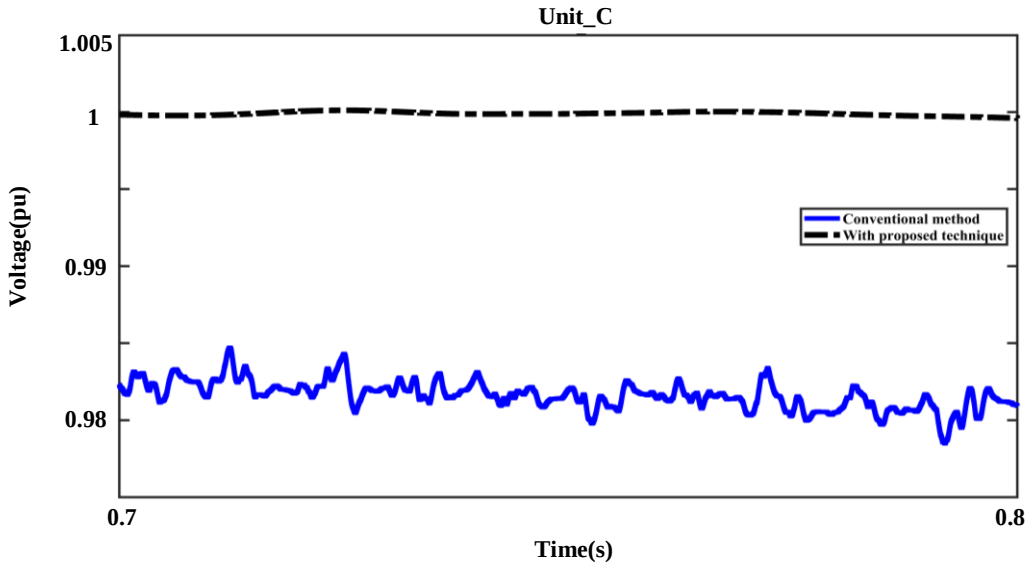

Fig.13. The open view of $unit_C$ voltage, with and without operating the proposed method

Among the units used in the system under study, $unit_C$ has the worst operating conditions under normal conditions. The output voltage of $unit_C$ in the form of a plot is shown in Fig.12. One of the reasons for the worst operation in this unit is the factor of the unbalanced nonlinear loads. As shown in the figure, the amplitude of the system voltage oscillation initially fluctuates from 0.0025pu to 0.0033pu. The oscillation amplitude and disturbances of the system will have a decreasing trend and finally, the voltage value of this unit will be stabilized at 0.98pu with an oscillation amplitude of 0.0033pu. As can be seen in Fig.13, considering the proposed method, in addition to increasing the system voltage by 0.02pu, the amplitude of voltage fluctuations is completely eliminated and the operation of $unit_C$ voltage is almost stable and without fluctuations.

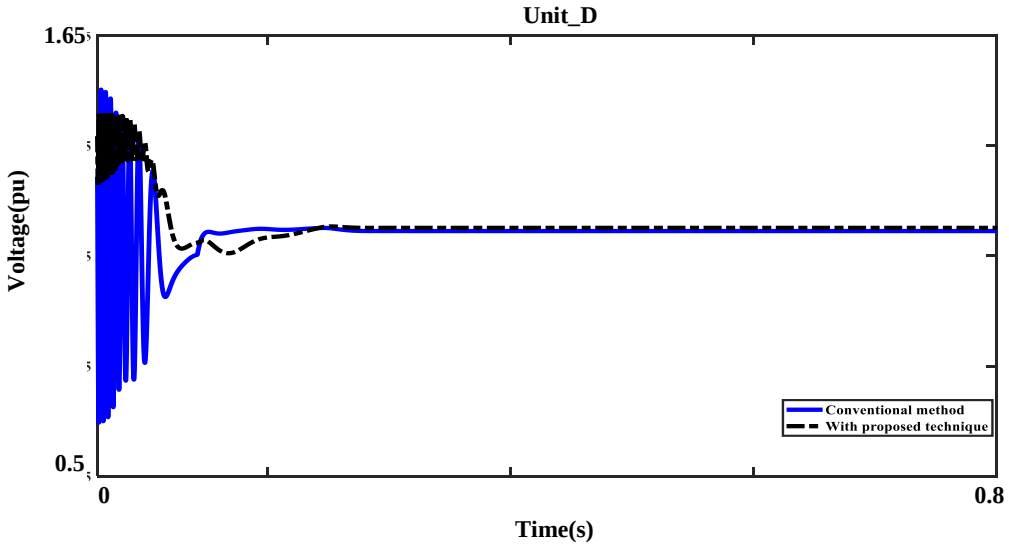

Fig.14. The voltage output of $unit_D$ with and without operating the proposed method

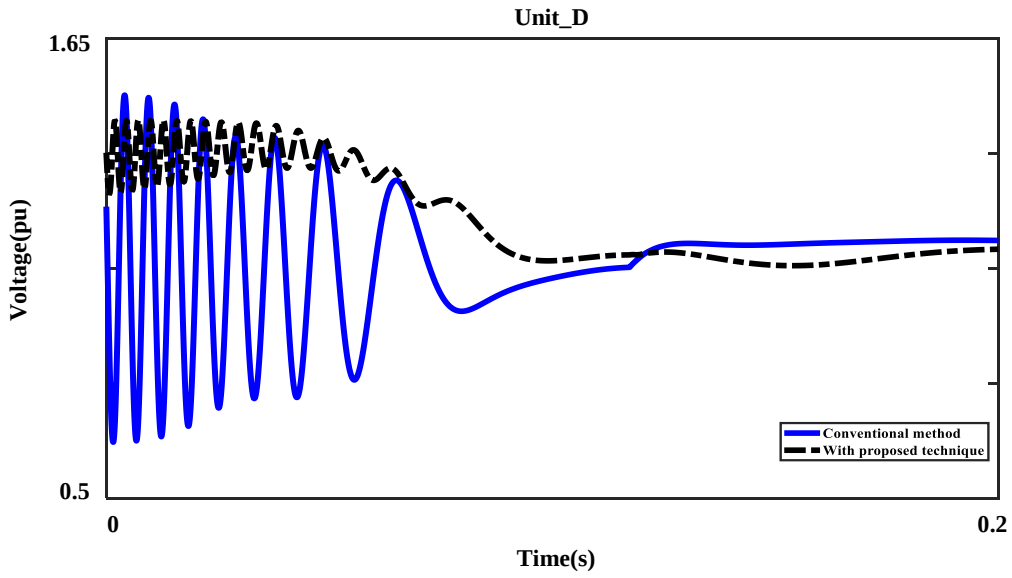

Fig.15. The open view of $unit_D$ voltage, with and without operating the proposed method

In $unit_D$, unlike the previous unit ($unit_C$), the situation of operating conditions seems to be relatively more profitable (except for the initial moment), which also depends on the loads' nature and the operation performance. According to the output of the voltage component plot shown in Fig. 14, the starting voltage will abnormally start with an oscillation (0.25pu to 1.45pu) and then stabilize at 0.94pu without any oscillation. Further, the range of fluctuations reduction is surely due to the change in operating conditions and the removal of some loads. By following the open view (0 to 0.2 seconds) of the unit voltage in Fig. 15, it seems that applying the proposed method, as in previous scenarios, in addition to increasing the system output voltage to 0.942pu, the voltage oscillation range in the initial moment has decreased significantly (according to the definition of limiting constraints). In order to better understand the proposed approach, the general pattern of improving the system voltage stability is as follows:

The FTCT works by ensuring that all generators in the unit reach a consensus voltage value in a finite amount of time. To achieve this, each generator in the system is considered an agent, and the method aims to control the voltage of each agent in such a way that all agents reach a consensus voltage value in a finite amount of time. it is achieved through a set of constraints that are designed to adjust the voltage of each agent based on the difference between its current voltage and the average voltage of all agents in the system. The constraint used in the proposed method is designed to ensure that the voltage of each agent converges to the consensus voltage value in a finite amount of time. This is achieved by incorporating a time-varying gain in the control law that helps to drive the voltage of each agent toward the consensus value. Recorded voltage values of each unit are presented in Table 3. The voltage oscillations range reduced between 0%-420% in the proposed method for each unit.

TABLE 3 The values of the units' output voltages

Kind of unit	Conventional method (pu)	With proposed method (pu)	Oscillation improvement (%)
Unit_A	0.985	1	150
Unit_B	0.99	1	400
Unit_C	0.98	1	420
Unit_D	0.94	0.942	0

After examining the first part of the problem, the topic of the system voltage dynamic behavior, the next problem, the system frequency dynamic behavior with conventional operating modes, and the proposed method will be examined. Fig. 16, shows the frequency behavior of $unit_A$ in various operating modes. In this plot, the amplitude of dynamic frequency oscillations is usually between 0.97pu to 1.17pu (oscillation=0.2pu), which is reduced to less than 0.01pu using the proposed method. The output view of the $unit_B$ operating frequency is shown in Fig. 17. As well, in

magnified parts (P1 and P2) the frequency of the desired unit is more clearly visible. In normal operation, the operating and behavioral conditions of the system frequency are almost the same. Observing the beginning of the operation (Part 1), it is clear that the operating frequency of this unit was out of range (0.96pu to 1.25pu). Then in this operating mode, the system frequency has an oscillation of 0.19pu, which will eventually stabilize the operating frequency at 1pu (Part 2). With the proposed method support, the operating conditions are relatively more favorable, and in addition to adjusting the operation of the unit at the nominal frequency, the amplitude of the system oscillations will be reduced to 0.012pu.

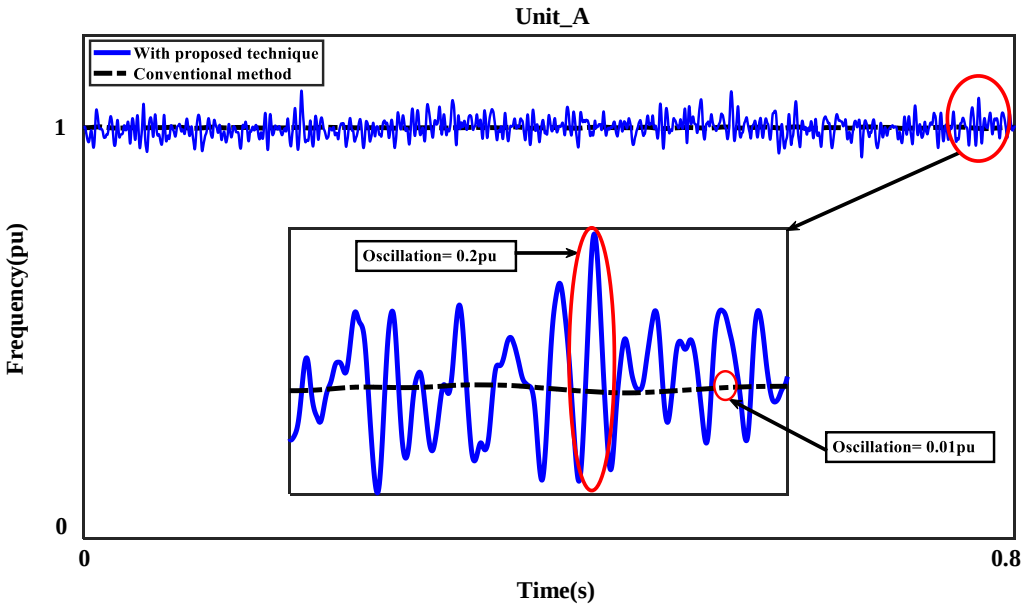

Fig.16. The $unit_A$ operate frequency with and without using the proposed method

Following, $unit_C$ operating frequency is shown in Fig. 18. The recorded view of this frequency (conventional mode) indicates the performance in the unauthorized area (oscillations 0.3pu). In the mentioned (conventional) operating mode, the oscillation amplitude is almost irregular, and as it is clear, in the enlarged view of this plot, the oscillation amplitude is 0.26pu, which has been reduced to 0.044pu by the proposed technique.

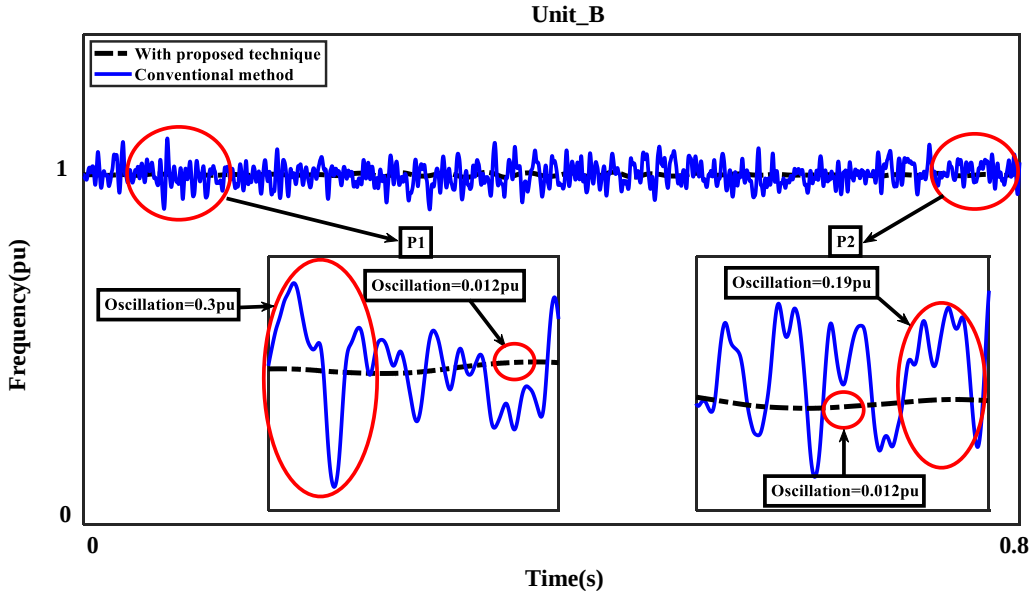

Fig.17. The $unit_B$ operate frequency with and without using the proposed method

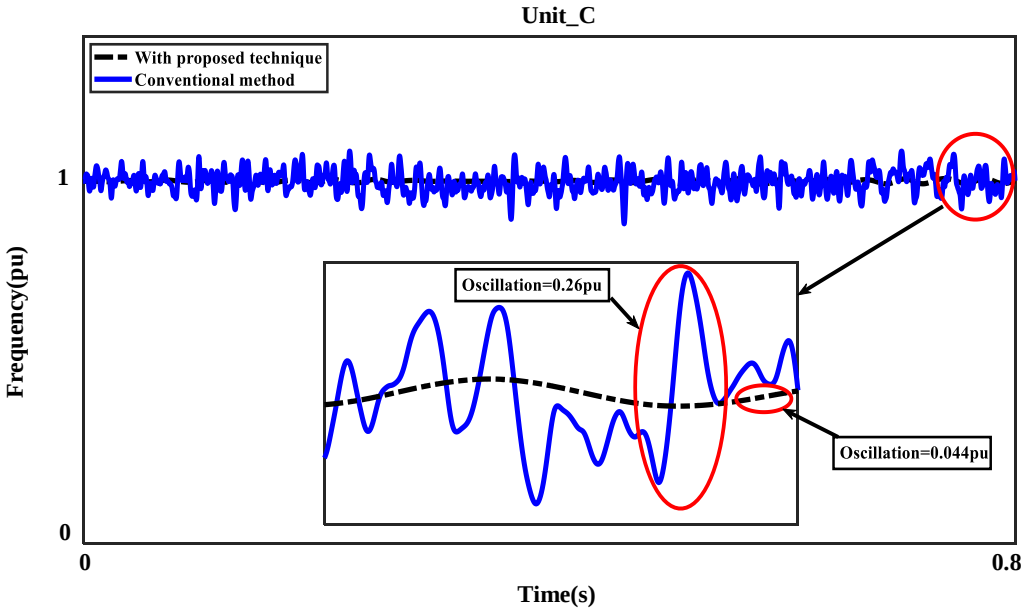

Fig.18. The $unit_C$ operate frequency with and without using the proposed method

Fig. 19, shows $unit_D$ output frequency. An oscillation with a value of 0.073pu (P1) occurs before 0.1 seconds, which is then damped. In the following, the unit in question has a relatively severe oscillation (change in operating conditions), which is often visible in the output with more limited amplitude fluctuations. Finally, the measured value of the frequency domain oscillation is 0.18pu (P2). Considering the proposed technique, the oscillations of the conventional method will be completely improved and the frequency value of the desired unit will be stabilized at 1pu. The measured frequency oscillation values of units are presented in Table 4.

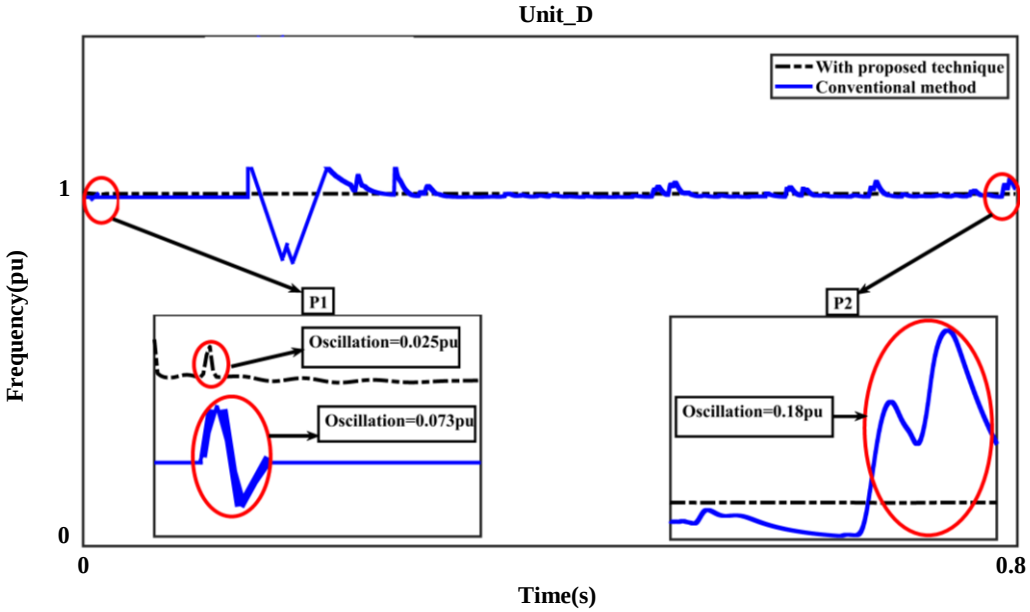

Fig.19. The $unit_D$ operate frequency with and without using the proposed method

The active and reactive powers of the studied system are shown in Figs. 20 and 21. The units' active powers are shown separately in Fig. 20. Due to the direct relationship and dependence of active power and frequency, the correct effect of the proposed method in damping and reducing power fluctuations to provide loads of each unit is known. In

the following, the power parameter values (P) of each unit, including $unit_A$, $unit_B$, $unit_C$, and $unit_D$, are fixed in the quantities of 0.9pu, 0.73pu, 0.36pu, and 0.52pu, respectively. Also, the reactive power obtained for each unit is presented in an overview in Fig. 21. The reactive power amplitude changes for all units in the initial moment are obvious, which have improved in subsequent cycles.

TABLE 4 The measured frequency oscillation values of units

Kind of unit	Conventional method (pu)	With proposed method (pu)
Unit_A	0.2	0.01
Unit_B	0.19	0.012
Unit_C	0.26	0.044
Unit_D	0.18	0

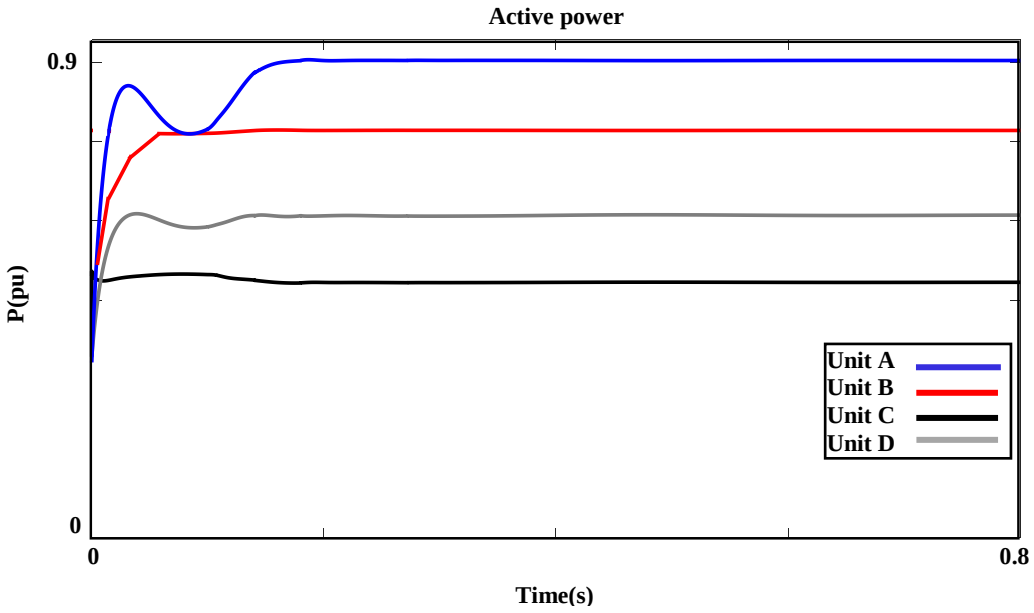

Fig.20. The active power of units

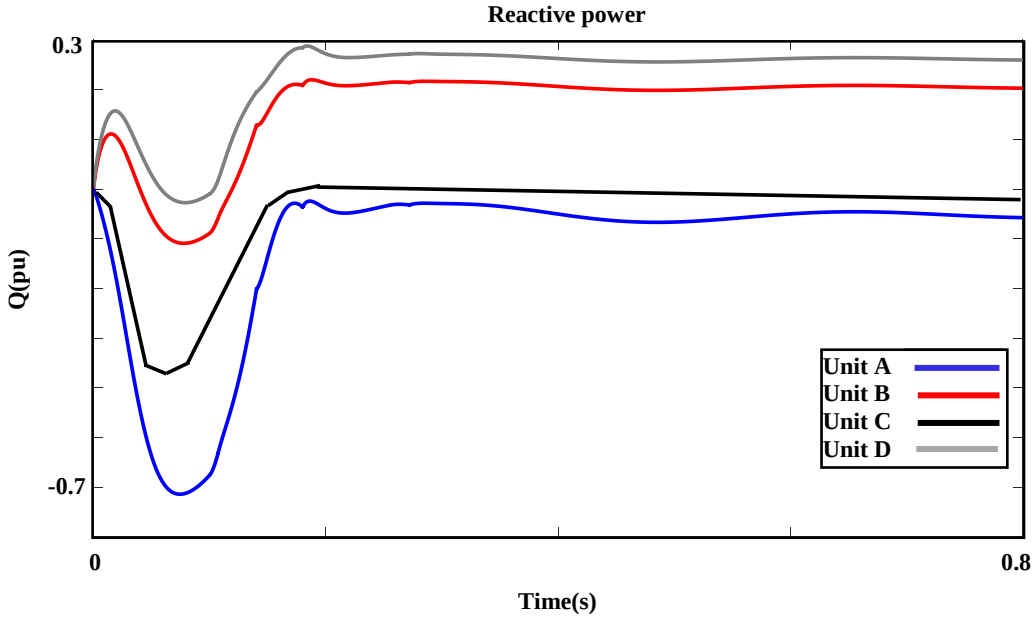

Fig.21. The reactive power of units

Finally, it can be concluded that the output ‘Q’ cannot be unaffected by the proposed method due to the direct relationship between the units' reactive power and voltage. The influence of different penetration levels of DERs on V/F stability depends on several factors such as the type and size of the DER, the DER location, and the control strategies used to manage the DER. At low penetration levels, DERs have minimal impact on V/F stability since they contribute a small portion of the total power supply. As the penetration level of DERs increases, their influence on V/F stability becomes more significant. One of the fundamental challenges associated with high levels of DER penetration is the variability and uncertainty of their output. For example, solar PVs and WTs are dependent on weather conditions and can experience rapid changes in output power. This variability can lead to V/F deviations in the power system if not managed properly. To mitigate the DER penetration impact at high levels, various control strategies can be employed. These include droop control, virtual inertia control, and frequency regulation control. Droop control is a decentralized control strategy that adjusts the output power of DERs based on local voltage and frequency measurements. Here, the applied DERs with droop control can have a significant influence on the stability and reliability of the power grid. The penetration level of DES refers to the percentage of total installed capacity that is made up of these sources. However, the functional and behavioral diagram of two control components (VDC, FDC) to describe the influence of different penetration levels of DERs is presented in Fig. 22. Overall, the influence of different penetration levels of DERs with PDC will depend on a range of factors, including the specific characteristics of the grid, the types of DER being used, and the control strategies being employed. To ensure the smooth integration of these sources, careful planning, and coordination will be necessary, along with ongoing monitoring and control.

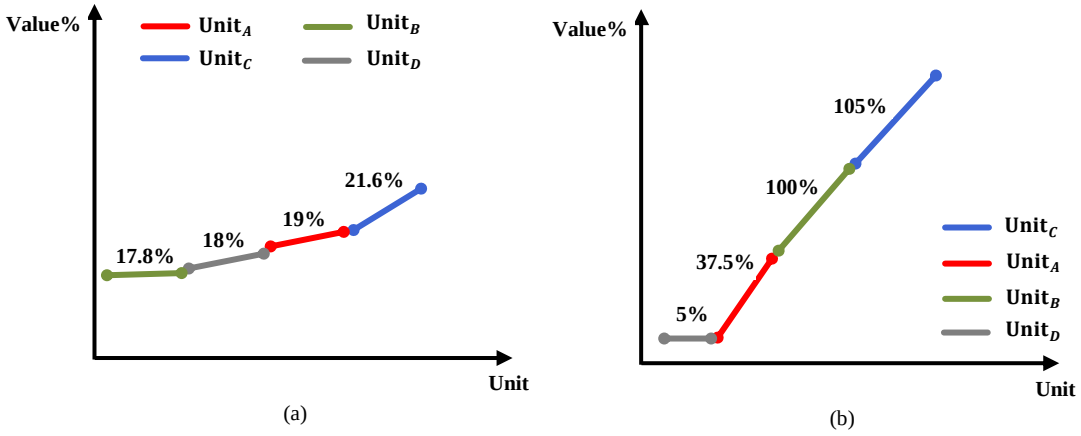

Fig.22. Influence investigation of different penetration levels of DERs by PDC (a) FDC mode (b) VDC mode

To better understand the proposed approach, the general pattern of improving the system frequency stability is as follows: The FTCT technique can be used to improve the coordination and response of multiple generators in the system. The method involves using a feedback control algorithm that enables the generators to communicate with each other and share information about their output power. The algorithm uses this information to adjust the generators' output power in a coordinated manner so that they all converge to a common value in a finite amount of time. This means that the generators will adjust their output power in response to changes in load demand or disturbances so that the system frequency remains stable and within acceptable limits.

In this section, the results of implementing the structure of the studied system in the software platform were executed. Two parameters of voltage and frequency dynamic behavior studies were performed in the form of separate scenarios on grid units. The output of each of these scenarios showed that the proposed control technique, at the secondary layer designed to return the system frequency and voltage to nominal values and compensate for a persistent error, is certainly useful. By applying the secondary controller designed in the units control structure, after the operation of VDC and FDC in the PDC is completed, the secondary control acts according to the defined goals (SVC

and SFC modes) and restores the units' voltage and frequency to the nominal values with minimum oscillation. Among the units, $unit_C$ with a variable amplitude of 0.26pu had the worst operating conditions in normal mode, which was achieved by using the proposed method of the best technical feedback. Regarding the issue of system voltage, $unit_C$ with the worst operating conditions (oscillation range 0.0025pu to 0.0033pu) was able to improve its working conditions to the most desirable way (420%) with support of the proposed method. The following are the nominal values of 'P' and 'Q' in Table 5.

TABLE 5 The units active and reactive power output

Kind of unit	Active power (pu)	Reactive power (pu)
Unit_A	0.9	-0.05
Unit_B	0.73	0.2
Unit_C	0.36	-0.02
Unit_D	0.52	0.28

5. Conclusion

Frequency and voltage stability are critical factors for the reliable operation of any power system, including HMGs. This paper studied the problem of controlling HMGs based on DERs. A two-layer interactive control scheme was developed for ensuring the voltage and frequency stabilities under different operating conditions. The proposed method has introduced two control modes including VDC and FDC in the first layer (PDC) to adjust the units V/F. The second layer is based on two modes (SFC and SVC), using the FTCT technique. The simulation results prove the efficiency of the proposed technique in the V/F control as the V/F components oscillations domain of the units has decreased to a considerable value. Furthermore, the values of improving the amplitude of oscillations and fluctuations for V/F components vary from 0.02pu-0.2pu and 0.178pu-0.216pu, respectively. Finally, with the development of MGs, sustainability issues such as load balancing, quality of power supply, renewable energy integration, and grid stability for mentioned systems in the form of novel control methods can be practical for new study opportunities in the future.

References